Supporting Information

Impact of physico-chemical heterogeneity on arsenic sorption and reactive transport under water extraction

Yanhua Duan[†,‡,#], Rong Li[‡,#] Yiqun Gan[†], Kai Yu[‡], Jiarong Tong[†,‡], Guangci Zeng[‡], Dongfang Ke[‡], Wenxian Wu[‡], Chongxuan Liu*[,‡]

[†] School of Environmental Studies, China University of Geosciences, 430074 Wuhan, China

[‡] School of Environmental Science & Engineering, Southern University of Science and Technology, 518055 Shenzhen, Guangdong, China

* Corresponding author: Chongxuan Liu (email: liucx@sustech.edu.cn; postal address: 1088 Xueyuan Road, Nanshan District, Shenzhen, Guangdong, China)

[#] Yanhua Duan and Rong Li contribute equally to this article

Pages: 13

Tables: 4

Figures: 12

Table S1 Chemical compositions of the sand and clay used for the flume experiment

	Na_2O	MgO	Al_2O_3	SiO_2	K_2O	CaO	Fe_2O_3	P	Ti	Mn	Ni	Ba
	%							ppm				
Clay	0.4	3.6	7.5	78.2	1.0	1.8	2.5	210	989	178	355	321
Sand	SiO_2											

Note: elements with the content less than 100 ppm were no listed in the table.

Table S2 The particle size, permeability, dispersivity, and initial sorption distribution coefficient for each zone in the flume.

	Layer 1	Layer 2	Layer 3	Layer 4-5, prefer. flow paths	Clay layers, clay lens
Particle size (μm)	75	100	150	300	-
Permeability (m^2)*	1.16×10^{-12}	2.07×10^{-12}	4.66×10^{-12}	1.86×10^{-11}	5.17×10^{-15}**
Dispersivity	$D_L=10^{-3}$ m, $D_T=10^{-4}$ m for all zones				
Initial sorption distribution coefficient K_d (mL/g)	1.38	0.27	1.40	0.39	5.65

* The permeability for sand layers and the preferential flow paths was calculated based on Kozeny-Carman equation.

** Clay permeability was obtained from sensitivity analysis.

Table S3 Parameters used in linear sorption model (K_d) and the dual first-order kinetic sorption model (f_1, f_2, k_1, and k_2).

	K_d (ml/g)	f_1	f_2	k_1 (h^{-1})	k_2 (h^{-1})
Mixed clay	5.65	0.89	0.11	118.07	0.23
Sand-1 (300 μm)	1.38	0.56	0.44	1.31	27.50
Sand-2 (150 μm)	0.27	0.46	0.54	16.13	1.64
Sand-3 (100 μm)	1.40	0.58	0.42	1.26	25.13
Sand-4 (75 μm)	0.39	0.48	0.52	19.24	1.38

Note that $f_1 + f_2 = 1$, therefore, only three parameters were independent in the dual first-order kinetic sorption model.

Table S4 The relative contents of Fe(II) and Fe(III) in the clay materials sampled before and after the flume experiment as determined using X-ray photoelectron spectroscopy.

		Fe (II)		Fe(III)	
		%	Binding energy (eV)[3-6]	%	Binding energy (eV)[3-6]
Clay - before experiment		29	709.8	71	711.4 and 713.4
Clay1		17	709.5	83	711.3 and 713.4
Clay2	After	23	709.7	77	711.5 and 713.4
Clay3	experiment	22	709.5	78	711.3 and 713.4
Clay4		19	709.5	81	711.3 and 713.4

Note: Clay1 to Clay4 were the clay samples collected from different positions in the flume.

Grain-scale kinetic model.

A dual first order kinetic sorption model was used to describe the kinetic sorption of As to the grains:[1,2]

$$\frac{dq_{t,i}}{dt} = k_i(q_{e,i} - q_{t,i}) \quad (i = 1, 2) \qquad \text{(S1)}$$

$$q_{e,i} = K_d * C_{aq} * f_i \qquad \text{(S2)}$$

$$q_t = q_{t,1} + q_{t,2} \qquad \text{(S3)}$$

where t is the contact time during the sorption experiments (h), k_i (h^{-1}) is the first-order rate constant at sorption site i, f_i is the site fraction for site i, K_d (L/g) is the linear equilibrium sorption constant, C_{aq} (μg/L) is the aqueous As concentration, $q_{t,i}$ (μg/g)is the actual sorbed amount of As at time t on site i, $q_{e,i}$ (μg/g) is the calculated sorbed amount of As at site i in equilibrium with C_{aq} at time t. The model parameters were determined by fitting the model to the experimental data (Fig. S1). K_d was estimated from the equilibrium sorption data in batch reactors.

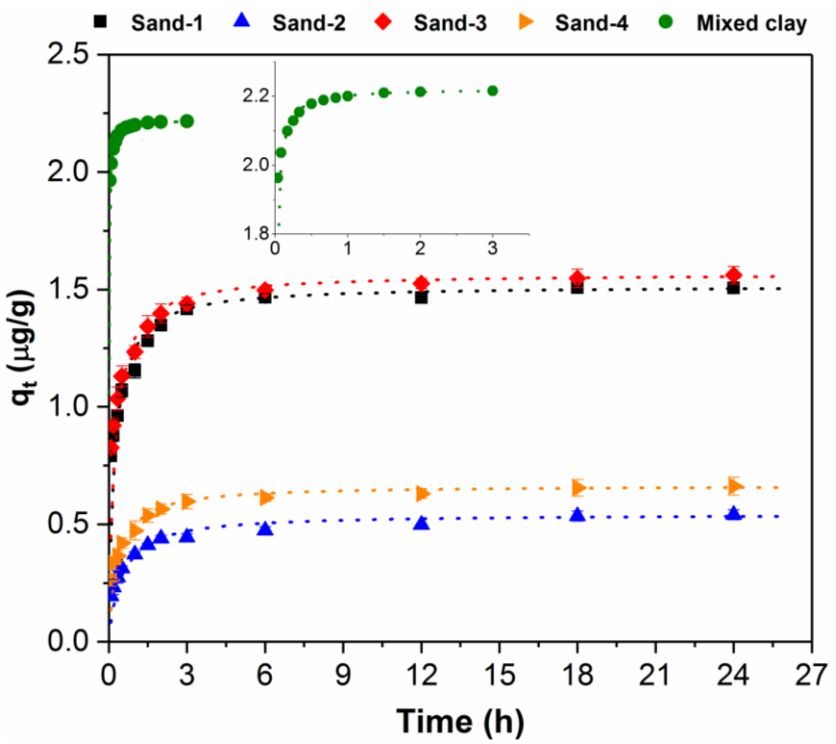

Figure S1 Measured As sorption as a function of time for the quartz sands and mixed clay materials in batch reactors. The data were used to determine the parameters in the dual first-order kinetic sorption model. In the plots, symbols denoted the measured data, and dash lines denoted the fitting results.

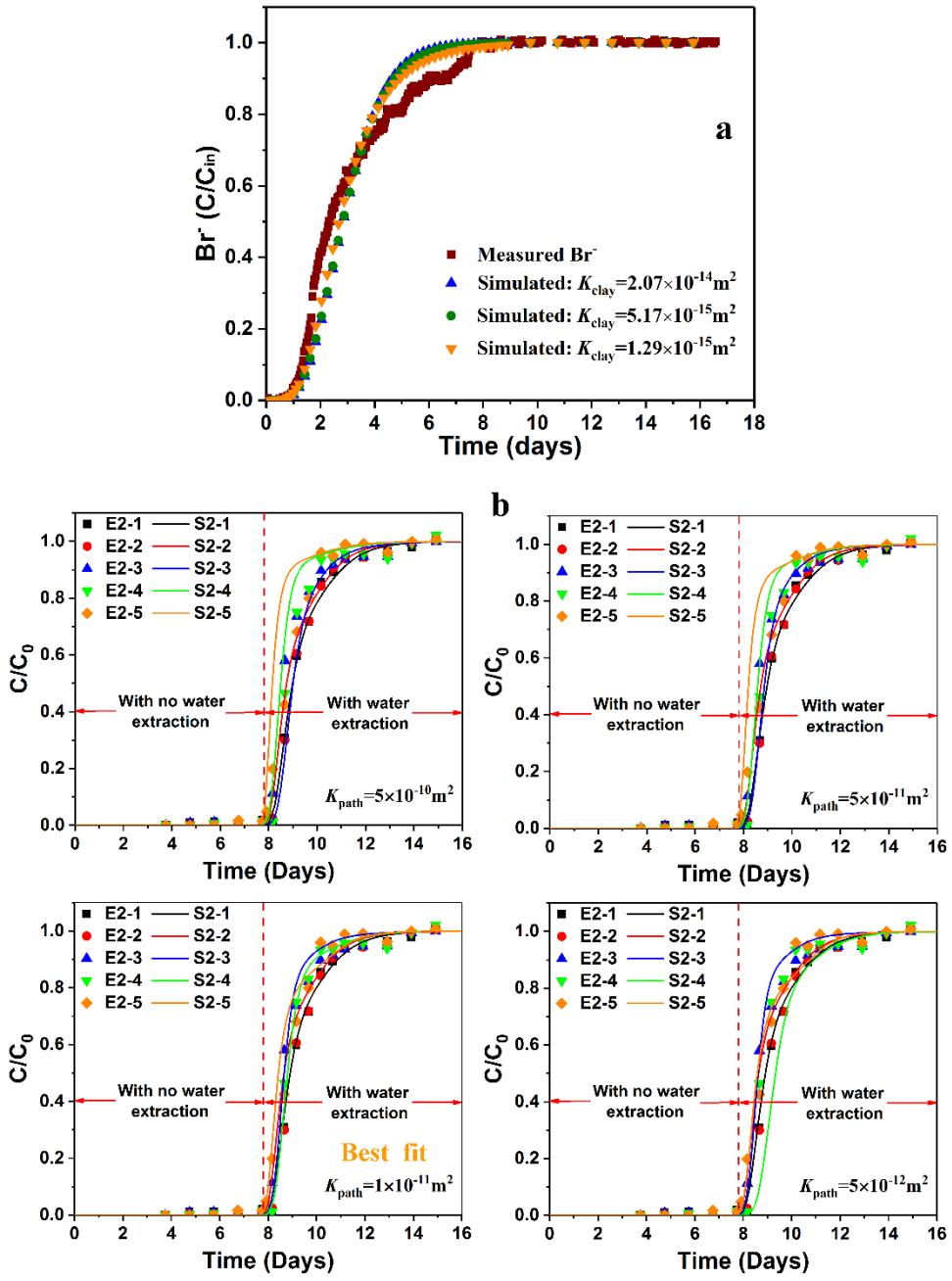

Figure S2 Sensitivity analysis results for (a) clay permeability (K_{clay}) vs. Br^- breakthrough curves at water extraction "well" and (b) preferential path permeability (K_{path}) vs Br^- breakthrough curves at sampling ports 2-1 to 2-5. In Fig. S2 (a), K_{clay} ranged from 1.29×10^{-15} to 2.07×10^{-14} m^2 and this range was calculated from the Kozeny-Carman equation with the possible particle size range (2.5 to 10 μm). The Br^- BTC was almost not affected by K_{clay} indicating the minor impact of K_{clay} on the flow and solute transport. In the simulation, we used 5.17×10^{-15} m^2 (corresponding to 5 μm size) as K_{clay} in Table S2.

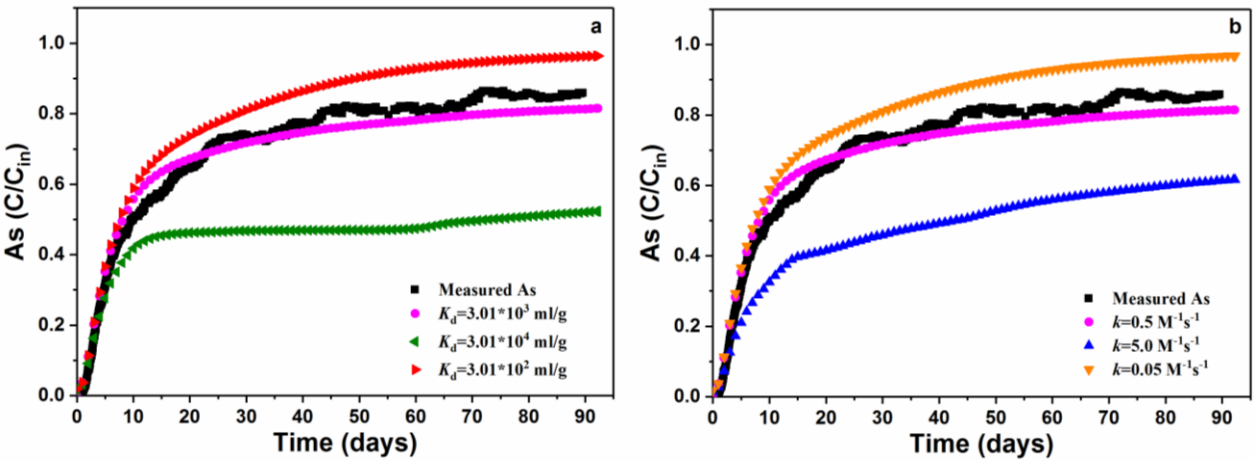

Figure S3 Results of sensitivity analysis for (a) K_d for As on newly formed Fe(III) and (b) $k_{Fe(II)}$ (rate constant for clay-bonded Fe(II) oxidation) on As breakthrough curves at water extraction "well".

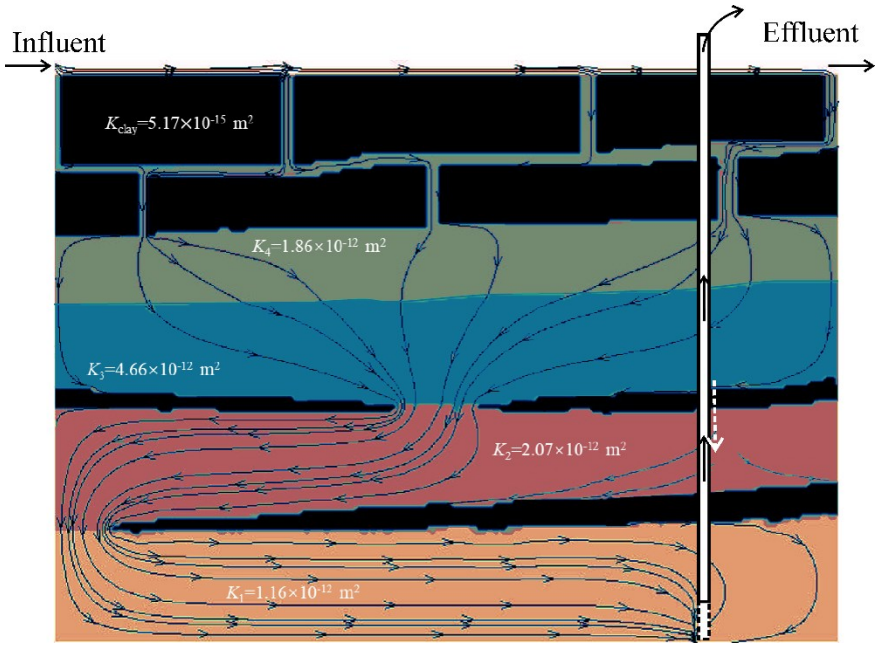

Figure S4 The distribution of permeability (color scale) and streamlines (arrow lines) in the flume. The white dash arrow near the well pipe denoted the unintended invisible preferential flow path in the clay lens.

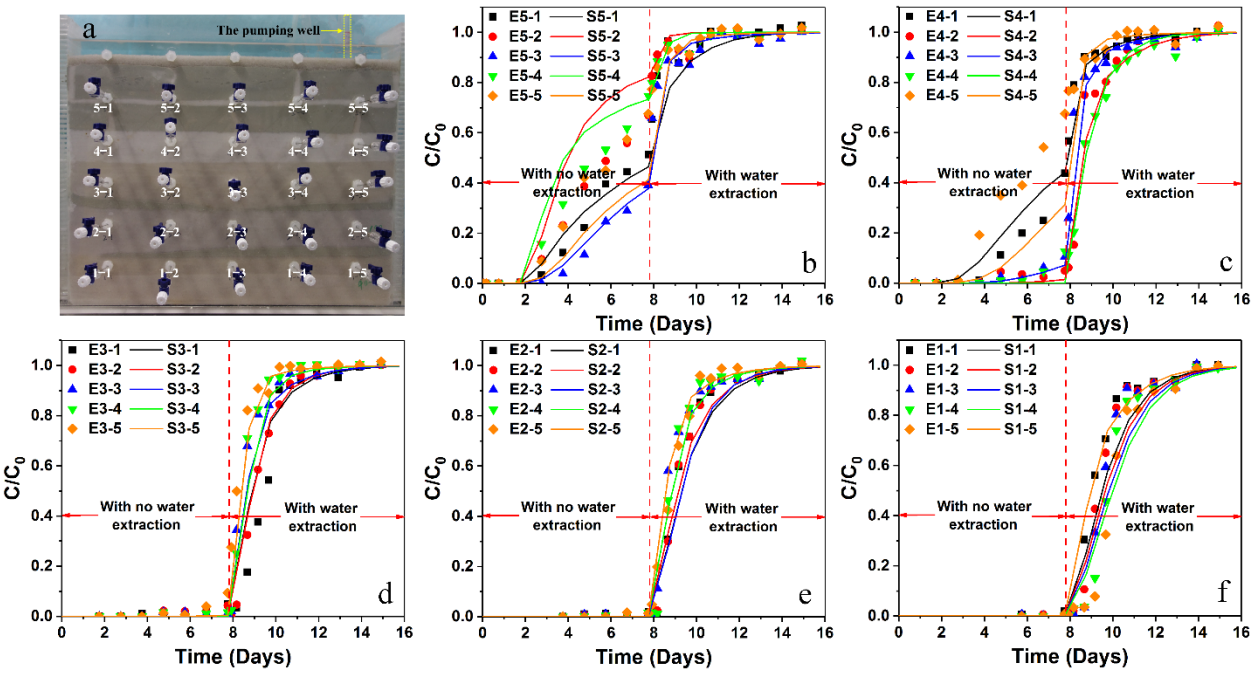

Figure S5 Breakthrough curves of Br concentrations at different sampling ports. a, the packed flume and the distribution of sampling port (e.g. 5-1, 1-1 etc.) ; b-f, changes of Br concentration at the sampling locations as a function of time. Solid symbols denoted the experimental results (labeled with E followed by sampling port number), and lines denoted the simulated results (labeled with S followed by sampling port number). The vertical dash lines showed the start time (at day 7.75) of water extraction in the extraction "well".

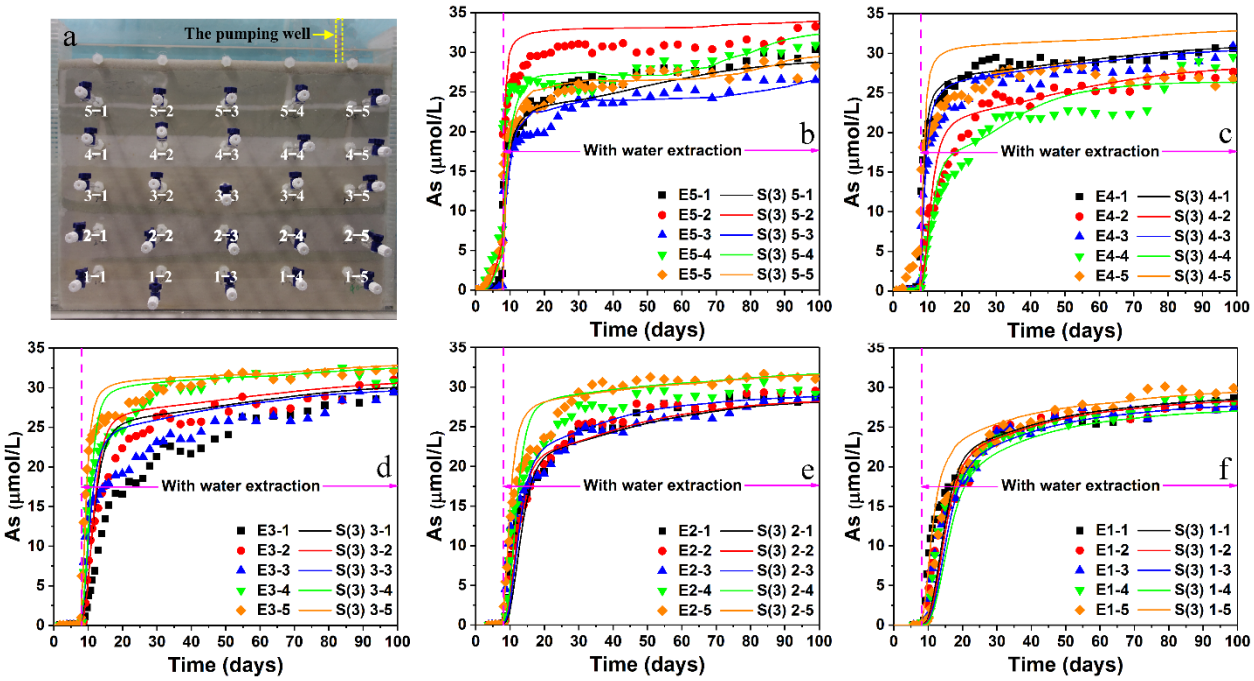

Figure S6 Breakthrough curves of As concentrations at different sampling ports. a, the packed flume and the distribution of sampling port locations; b-f, changes of As concentrations as a function of time at the sampling locations. Solid symbols denoted the experiment data (labeled with E followed with sampling port number), and lines denoted the simulated results at the sampling ports (labeled with S followed with sampling port number) using the reactive transport model with time-variable K_d model (Case 3). Arsenic concentration in the influent solution was 35 μM. Water extraction from the bottom extraction well started at day 7.75.

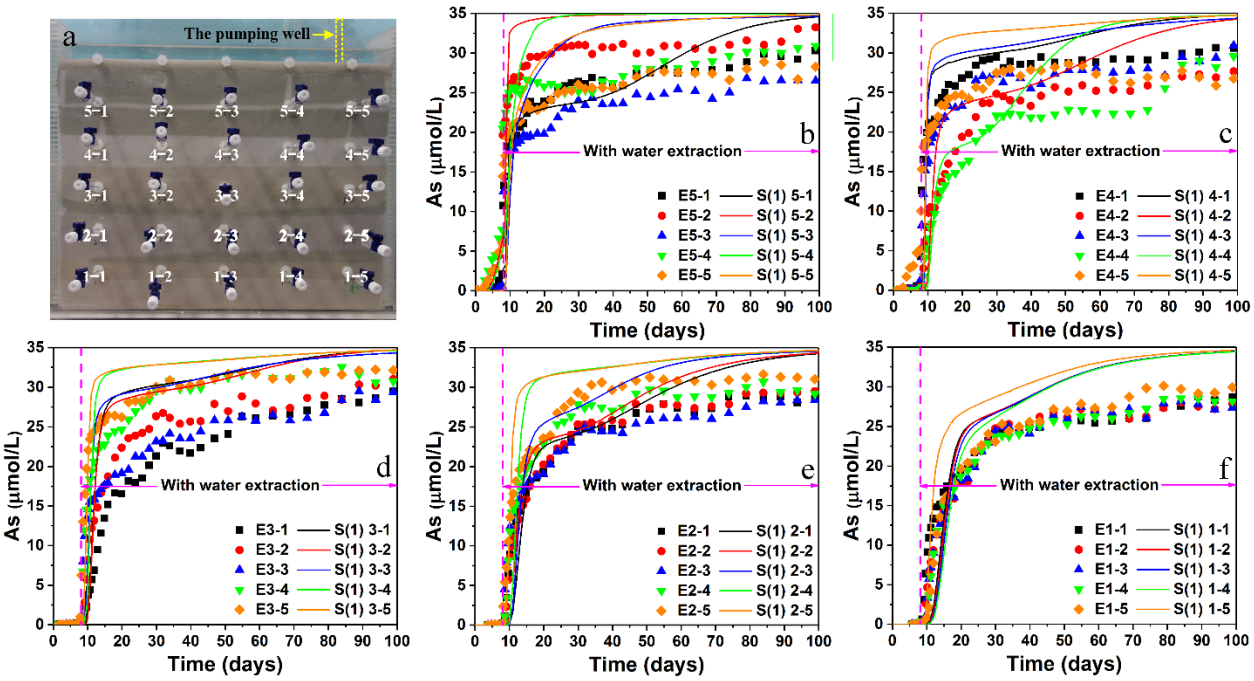

Figure S7 Breakthrough curves of As concentrations at different sampling ports. a, the packed flume and the distribution of sampling port locations; b-f, changes of As concentrations as a function of time at the sampling locations. Solid symbols denoted the experiment data (labeled with E followed with sampling port number), and lines denoted the simulated results at the sampling ports (labeled with S followed with sampling port number) using the reactive transport model with equilibrium sorption model (Case 1). Arsenic concentration in the influent solution was 35 μM. Water extraction from the bottom sand layer started at day 7.75.

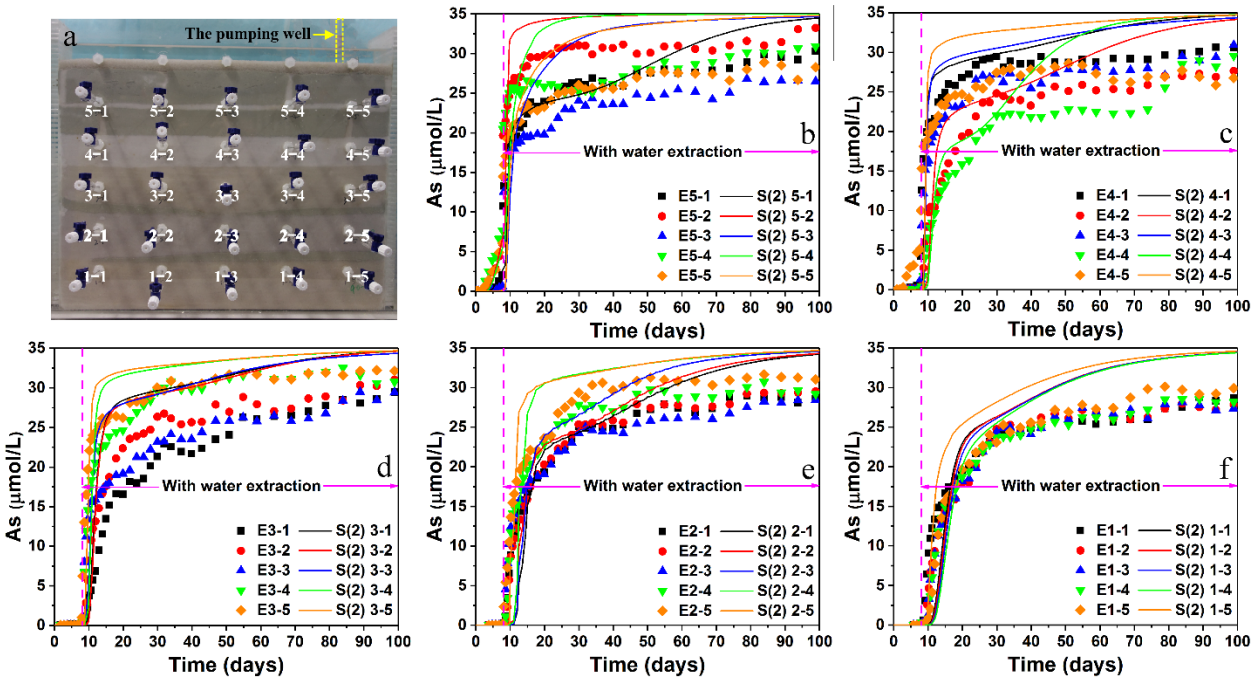

Figure S8 Breakthrough curves of As concentrations at different sampling ports. a, the packed flume and the distribution of the sampling port locations; b-f, changes of As concentrations as a function of time at the sampling locations. Solid symbols denoted the experiment data (labeled with E followed with sampling port number), and lines denoted the simulated results at the sampling ports (labeled with S followed with sampling number) using the reactive transport model with dual first-order kinetic sorption model (Case 2). Arsenic concentration in the influent solution was 35 μM. Water extraction from the bottom sand layer started at day 7.75.

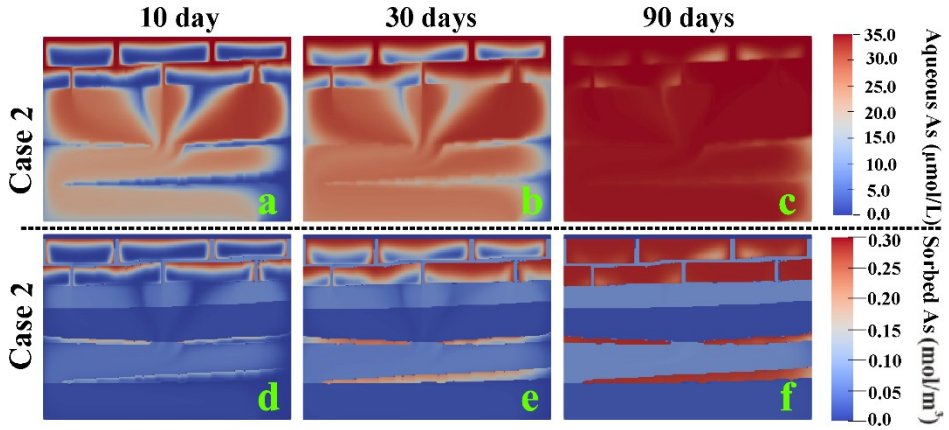

Figure S9 Simulated distributions of the total aqueous As (a-c) and the total adsorbed As in the flume (d-f) for Case 2.

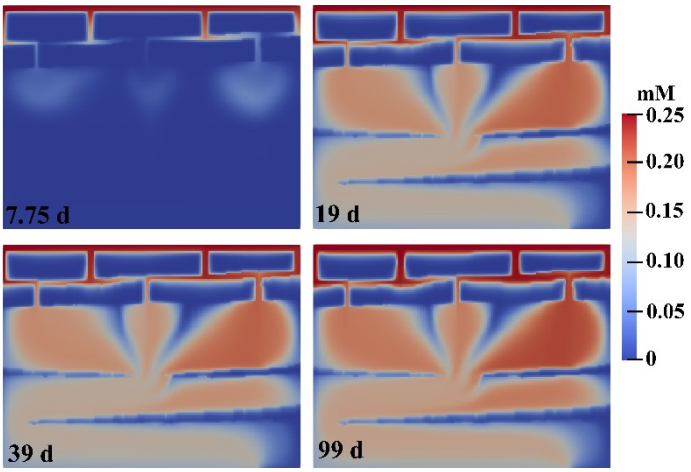

Figure S10 Simulated distributions of DO concentration for Case 3 (Table 2) in the flume at day 7.75 (the end of no water extraction period), 19, 39, and 99. The advection-dispersion based equation was combined with a consumption term determined by kinetic oxidation rate of clay-bonded Fe(II) to solved the reactive transport of DO in the flume system. Based on the electron balance, DO consumption rate can be calculated as $R_{DO} = 0.25R_{Fe(II)}$ ($R_{Fe(II)}$ was described in Eq. 2).

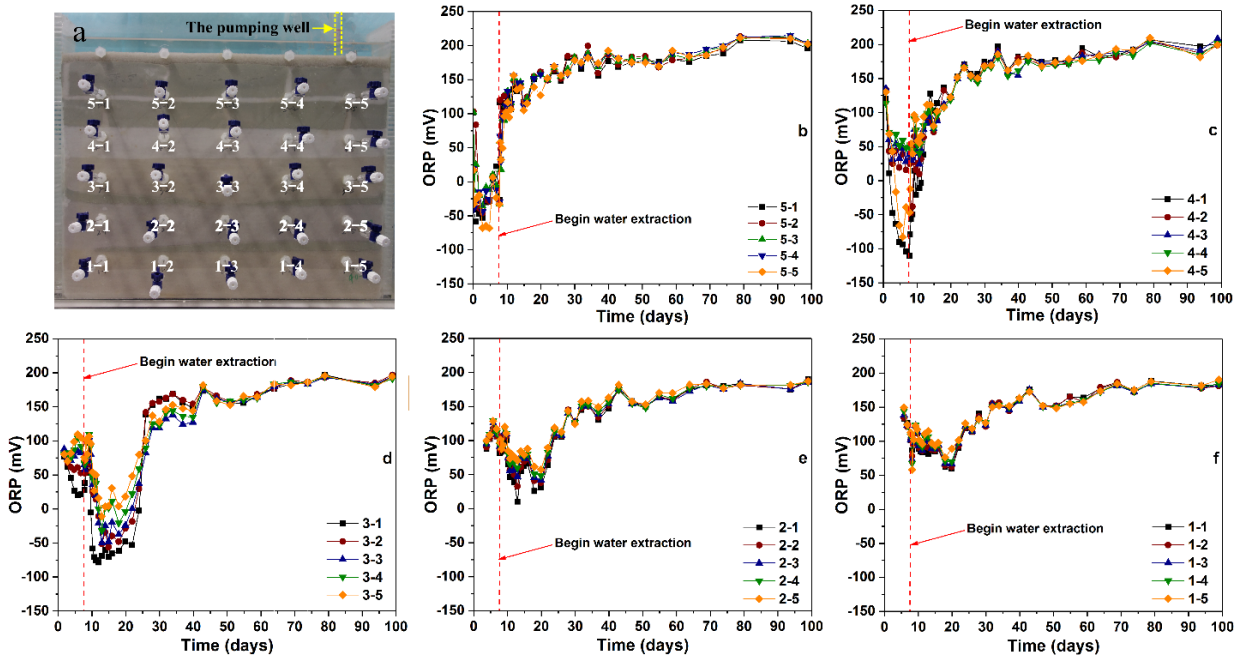

Figure S11 plot a, the packed flume and the distribution of the sampling port locations; plots b-f, changes of ORP values at different sampling locations. Water extraction from the bottom of the extraction "well" started at day 7.75.

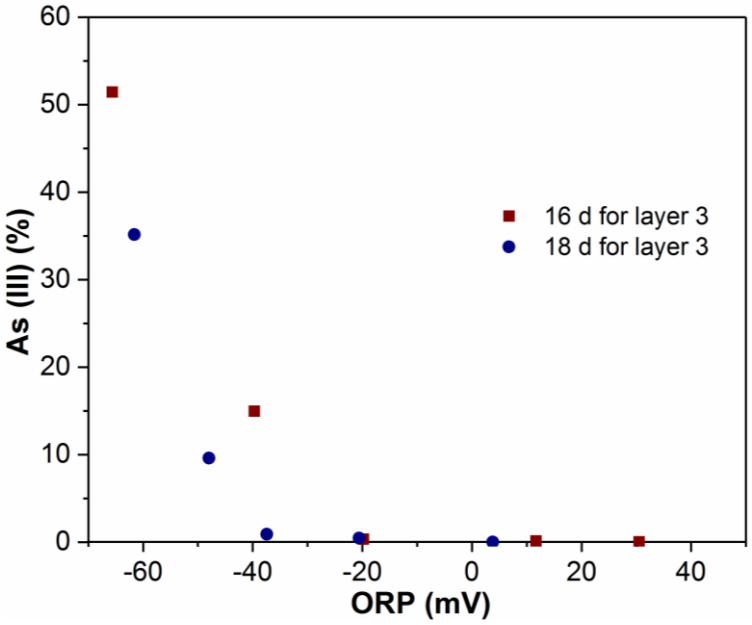

Figure S12 The relationship between the measured ORP values and percentage of As(III) in the aqueous samples collected from layer 3 at day 16 and 18

References

[1] Liu, C., Shi, Z., and Zachara, J.M., 2009. Kinetics of Uranium(VI) Desorption from Contaminated Sediments: Effect of Geochemical Conditions and Model Evaluation. Environmental Science & Technology, 43(17), 6560-6566.

[2] Ma, R., Zheng, C., Prommer, H., Greskowiak, J., Liu, C., Zachara, J.M., & Rockhold, M.L., 2010. A field‐scale reactive transport model for U(VI) migration influenced by coupled multirate mass transfer and surface complexation reactions. Water Resources Research, 46(5).

[3] Liao, P., Pan, C., Ding, W.Y., Li, W.L., Yuan, S.H., Fortner, J.D., Giammar, D.E., 2020. Formation and transport of Cr(III)-NOM-Fe colloids upon reaction of Cr(VI) with NOM-Fe(II) colloids at anoxic-oxic interfaces. Environmental Science & Technology, 54, 4256-4266.

[4] He, L., Xie, L., Wang, D., Li, W., Fortner, J.D., Li, Q., Duan, Y., Shi, Z., Liao, P., Liu, C., 2019. Elucidating the role of sulfide on the stability of ferrihydrite colloids under anoxic conditions. Environmental Science & Technology, 53, 4173-4184.

[5] Pratt, A. R.; Nesbitt, H. W.; Muir, I. J., 1994. X-ray photoelectron and Auger spectroscopic studies of pyrrhotite and mechanism of air oxidation. Geochimmica et Cosmochimica Acta, 58, 827-841.

[6] McIntyre, N. S. and Zetaruk, D. G., 1977. X-ray photoelectron spectroscopic studies of iron oxides. Analytical Chemistry, 49, 1521-1529.